Journal of Quaternary Science

Timing of glacial retreat in the Wicklow Mountains, Ireland, conditioned by glacier size and topography

Journal:	*Journal of Quaternary Science*
Manuscript ID	JQS-17-0106
Wiley - Manuscript type:	Research Article
Date Submitted by the Author:	23-Nov-2017
Complete List of Authors:	Tomkins, Matt; University of Manchester School of Environment and Development, Dortch, Jason; University of Manchester School of Environment and Development Hughes, Philip; University of Manchester School of Environment and Development Huck, Jonny; University of Manchester School of Environment and Development Tonkin, Toby; University of Derby, Department of Natural Sciences Barr, Iestyn; Manchester Metropolitan University, School of Science and the Environment
Keywords:	Schmidt Hammer exposure dating (SHED), Wicklow, Ireland, Glacier chronology, Topographic controls, ¹⁰Be dating

Timing of glacial retreat in the Wicklow Mountains, Ireland, conditioned by glacier size and topography

Matt D. Tomkins*, [1] Jason D. Dortch, [1] Philip D. Hughes, [1] Jonny J. Huck, [1] Toby N. Tonkin[2] and Iestyn D. Barr [3]

*Corresponding author (matthew.tomkins@postgrad.manchester.ac.uk)

[1]Department of Geography, School of Environment, Education and Development, The University of Manchester, Manchester, M13 9PL, UK

[2]Department of Natural Sciences, University of Derby, Kedleston Road, Derby, DE22 1GB, UK

[3]School of Science and the Environment, Manchester Metropolitan University, Chester Street, Manchester, M1 5GD, UK

Abstract

This paper presents 170 Schmidt Hammer exposure ages from moraine boulders and glacially-sculpted bedrock to reveal the post-Last Glacial Maximum (LGM) history of the Wicklow Mountains, Ireland. These data suggest that large ice masses survived for 4-7 ka after retreat of the Irish Sea Ice Stream and were sustained by summit ice-fields until ~16.6 ka. Post-LGM retreat was dynamic, with re-advance moraines deposited in response to Heinrich Stadial 1. However, these events reflect short-term ice front oscillations (≤ 1 ka) during the long-term retreat phase. Retreat from re-advance positions was synchronous across the range and paced by climate, with time-progressive deglaciation from low to high elevation. In contrast, marked asynchroneity in the timing of Younger Dryas deglaciation is closely linked to snow redistribution and indicates that for small cirque glaciers (≤ 1 km^2), topography can exert the primary control on glacier survival. This result has important implications for palaeoclimate reconstructions as cirque glacier dynamics may be unrelated to climate. This is further complicated by post-depositional processes which can result in moraine ages (e.g. ^{10}Be) which post-date retreat. Future palaeoclimate studies should prioritise cirque glaciers where snow contributing areas are small and where post-depositional disturbance is limited (matrix-poor, boulder-rich moraines).

Keywords

- Schmidt Hammer exposure dating (SHED)
- Wicklow, Ireland

- Glacier chronology
- Topographic controls
- ^{10}Be dating

Introduction

Recent studies have focused on the retreat dynamics of the Irish Sea Ice Stream (ISIS) (Chiverrell et al., 2013; Smedley et al., 2017a), a major outlet of the British-Irish Ice Sheet (BIIS; Smedley et al., 2017b). The timing of ISIS retreat after the Last Glacial Maximum (LGM; 23.3 – 27.5 ka; Hughes and Gibbard, 2015) has important implications for the dynamics of terrestrial ice masses and, in particular, proximal mountain ice caps (Clark et al., 2012). In the Irish Sea Basin, ice caps centred on the mountains of Wales (Hughes et al., 2016), the Lake District (Wilson et al., 2013) and Wicklow, Ireland (Ballantyne et al., 2006) coalesced with the ISIS during the LGM and may have persisted after ISIS retreat. However, while the deglacial chronologies of the Welsh and Lake District ice caps are constrained by ^{10}Be, OSL and ^{14}C ages (Ballantyne et al., 2009; McCarroll et al., 2010; Glasser et al., 2012; Lloyd et al., 2013; Hughes et al., 2016; Smedley et al., 2017b), there is a paucity of geomorphological and geochronological evidence for post-LGM activity in the Wicklow Mountains. ^{10}Be ages from summits in Wicklow (Ballantyne et al., 2006) and the adjacent Blackstairs Mountains (Ballantyne and Stone, 2015) indicate summit deglaciation soon after the LGM (n = 5; 21.0 - 22.9 ka), while a single ^{36}Cl age from the Mottee Stone (~20 km SE of Lugnaquilla (925m) at 52.886993, -6.208196) indicates separation of mainland ice and the ISIS by 23.1 ± 2.2 ka (Bowen et al., 2002). This timeframe accords with Bayesian modelling of ice stream retreat, with the ISIS retreating ~80 km along the Irish coast during the interval 20.8 – 23.9 ka (Smedley et al., 2017b). Recent research has begun to establish the geomorphological context for deglaciation in the Wicklow Mountains (Knight et al., 2017). However with the exception of isolated ^{14}C (n = 2, 11.5 - 11.6 ka; Colhoun and Synge, 1980) and ^{36}Cl ages (n = 1; 17.9 ± 1.0 ka; Bowen et al., 2002) from Lough Nahanagan, the geochronology of the deglaciation of the Wicklow Ice Cap is poorly understood. To address this knowledge gap, this study presents 170 Schmidt Hammer (SH) exposure ages from cirque and valley moraines and from a summit overridden by ice at the LGM. These data provide new insights into the contrasting deglacial chronologies of the ISIS and the Wicklow Ice Cap and the climatic and topographic factors which conditioned post-LGM retreat.

Methods

To develop a deglacial chronology, sampling was focused on prominent moraines and boulder accumulations as these are the best geomorphological indicators of the dimensions of former mountain glaciers (Barr et al., 2017). Key sites along the main SW-NE axis of the mountain range were targeted for Schmidt Hammer exposure dating (SHED; Tomkins et al., 2016) including glacially-deposited boulders on prominent cirque moraines (>400 m) at Kelly's Lough, Lough Nahanagan, Mullaghcleevaun and Upper Lough Bray. These moraines exhibit good spatial coherence (Kirkbride and Winkler, 2012) as they are generally matrix-poor, boulder-rich and feature clearly defined moraine crests, although the outer cirque moraine at Lough Nahanagan is degraded (Colhoun and Synge, 1980). This moraine is ~1 km in length, broadly convex in cross-profile form and consists of unsorted granite, sand and gravel deposits with entrained glacially smoothed granite boulders (1 - 4 m diameter; Colhoun and Synge, 1980). Multiple nested moraines and boulder accumulations are preserved within the inferred YD glacial limit at each site, which conforms to a pattern of active oscillatory retreat (Bickerdike et al., 2017). In addition, samples were obtained from valley moraines (250 – 400 m, c. 2 - 4 km from cirque headwalls) at Carrawaystick Brook, Upper Glendasan, Lough Brook and Glenmacnass Waterfall and from ice-moulded bedrock and erratic boulders from the summit of Carrigshouk (571 m), which was overridden by ice at the LGM (Fig. 1; Table 1). 20 surfaces were sampled at each site (Carrawaystick Brook; n = 10) and 170 surfaces were sampled in total, comparable to previous applications of SHED in the Mourne Mountains, Northern Ireland (Barr et al., 2017).

30 R-values were generated per surface (Niedzielski et al., 2009). Sampled boulders were of sufficient size (> 25 kg; Sumner and Nel, 2002; Demirdag et al., 2009) and all sampled surfaces were free of surface discontinuities (Williams and Robinson, 1983) and lichen (Matthews and Owen, 2008). *Instrument calibration* (Correction Factor = 1.017) and *age calibration* (Correction Factor = 0.992) were performed using the SHED-Earth online calculator (http://shed.earth) following the recommendations of Dortch et al. (2016). SH exposure ages and 1σ uncertainties were calculated based on the arithmetic mean for each surface (Mean of 30 R-values) and based on the updated calibration curve of Tomkins et al. (2017) which includes ^{10}Be dated surfaces from Blackstairs Mountain, Wexford (n = 2; Ballantyne and Stone, 2015) and Bloody Foreland, Donegal (n = 6; Ballantyne et al., 2007; Clark et al., 2009). These data fit the trend established at calibration sites in Scotland and NW England and indicate that errors in SH exposure age estimates due to climatic variability appear unlikely (Barr et al., 2017). Calibration site exposure ages are calculated using the online calculators formerly known as the CRONUS-Earth online calculator (http://hess.ess.washington.edu/math/, Wrapper script 2.3, Main calculator 2.1, constants 2.3, muons 1.1; Balco et al., 2008) and are based on the time-dependent Lm scaling (Lal, 1991; Stone, 2000), the Loch Lomond Production Rate (LLPR; Fabel et al., 2012; 4.02 ± 0.18 atoms g^{-1} a^{-1}) and assuming 0 mm ka^{-1} erosion. The LLPR is constrained by independent ^{14}C ages (MacLeod et al., 2011) and is the most widely used local production rate in the British Isles. However, the results presented here will be subject to recalibration in light of future refinement of local production rates. For each sampled site (n = 9), probability density

estimates (PDEs) were produced and modelled to separate out the highest probability Gaussian (Fig. 2; Dortch et al., 2013) to account for geological uncertainty. This analytical method has been employed in studies using ^{10}Be (Dortch et al., 2013; Murari et al., 2014) to identify ages that are too young (*moraine degradation*; Heyman et al., 2011) or too old (*inheritance*; Hallet and Putknonen, 1994).

Based on the results of SHED, three dimensional reconstructions of cirque glaciers were generated using the GLaRe tool (Pellitero et al., 2016; Basal shear stress = 100 kPa; Step length = 10 m) and used to estimate palaeo equilibrium-line altitudes (ELAs). Valley glaciers were also reconstructed for individual catchments using this method although ELAs were not calculated for these ice configurations as geochronological data are not available for all glacier outlets. ELAs were estimated using the GIS tool of Pellitero et al. (2015), applying the area-altitude balance ratio method (AABR = 1.9 ± 0.81; Rea, 2009). ELAs are controlled by climate (Ohmura et al., 1992; Hughes and Braithwaite, 2008) but are also strongly influenced by non-climatic factors (Table 2), such as the supply of snow and ice from indirect sources (Mitchell, 1996; Kern and Laszlo, 2010). To assess the impact of 'redistributed' snow and ice, combined snow and avalanche contributing areas (A_c) were calculated (c.f. Ballantyne, 2007a,b; Barr et al., 2017; Dominant wind direction W/SW = 210 - 300°, Avalanche slopes ≥ 25°) and compared to total glacier surface areas (A_g). The A_c/A_g ratio is a proxy for the potential contribution of redistributed snow to glacier accumulation.

Results

Gaussian SH exposure ages (Table 1) are in correct stratigraphic order in individual glacier catchments, are broadly consistent with comparable deglacial chronologies across the British Isles (Clark et al., 2012), and clearly differentiate cirque and valley moraines, with deposition during the Younger Dryas (YD; 11.7 - 12.9 ka) and Oldest Dryas respectively (GS-2.1a; 14.7 - 17.5 ka). Moreover, these datasets are chronologically robust (Kirkbride and Winkler, 2012), with well-dated moraine sequences in Glenmalur, Glendasan and Glenmacnass (Fig. 1), and provide a framework for a wider morphostratigraphic deglacial chronology for the Wicklow Mountains (Knight et al., 2017). At cirque sites, SHED indicates deglaciation by 12.31 ± 0.51 ka at Upper Lough Bray (ULB), 12.00 ± 0.44 ka at Kelly's Lough (KL), 11.40 ± 0.13 ka at Mullaghcleevaun (MC) and 10.93 ± 0.26 ka for the outer moraine at Lough Nahanagan (LN; Colhoun and Synge, 1980). In contrast, valley moraines were deposited at 16.46 ± 0.58 ka at Glenmacnass Waterfall (GW), 16.21 ± 0.60 ka at Upper Glendasan, 15.48 ± 0.35 ka at Carrawaystick Brook (CB) and 15.41 ± 0.30 ka at Lough Brook (LB). Finally, SHED indicates the emergence of Carrigshouk (CS) by 16.64 ± 0.82 ka. This date provides a minimum age for wider summit deglaciation in the Wicklows Mountains due to its comparatively low elevation (571 m) and central position on the range divide. Reconstructed cirque glaciers (Table 2) range in size from 0.35 km^2 (ULB) to 1.10 km^2 (LN) while snow contributing areas (A_c) range

from 0.12 km^2 (ULB) to 1.07 km^2 (LN). At Lough Nahanagan and Mullaghcleevaun, extensive upland plateaus to the west and south (210 - 300°) account for large snow contributing areas ($A_c \geq 1$ km^2). In contrast, restricted upslope areas within the glacier drainage basin likely limited the potential for significant snow redistribution ($A_c \leq 0.5$ km^2) at Kelly's Lough and Upper Lough Bray. AABR ELAs for cirque glaciers range from 513 m (LN) to 648 m (KL) and show no clear spatial clustering. Finally, reconstructed valley glaciers range in size from 4.96 km^2 (UGD) to 12.46 km^2 (GW) and demonstrative a progressive reduction in total glacier area (A_g) throughout the period 15.4 - 16.5 ka.

Discussion

Firstly, these data demonstrate that significant ice masses persisted in the Wicklows after retreat of the ISIS, with large valley glaciers (Length: ~4 km, Area: ~12.5 km^2) present until the onset of the Late-glacial (Greenland Interstadial-1; Rasmussen et al., 2014). While lowland (23.1 ± 2.2 ka; Bowen et al., 2002) and summit deglaciation (n = 3; 21.0 – 21.9 ka; Ballantyne et al., 2006) was coeval with ISIS retreat (Smedley et al., 2017b), SH exposure ages from the summit of Carrigshouk (571 m) indicate that summit ice fields were present on the range divide until 16.64 ± 0.82 ka. However, distal summits were ice free as early as 21.9 ± 1.1 ka (Djouce Mountain, 725 m), 21.2 ± 1.1 ka (Scarr, 641 m) and 21.0 ± 1.1 ka (Kanturk, 523 m) and evidence a significant time lag in summit deglaciation (~4.4 ka). Collectively, ^{10}Be and SHED ages indicate rapid downwastage of the Wicklow Ice Cap soon after the LGM and a transition to summit ice fields which sourced discrete outlet glaciers (e.g. Glenmacnass, Glendasan, Glenmalur; Fig. 1). This chronology is consistent with ^{10}Be ages from summits in Wales (Glasser et al., 2012; Hughes et al., 2016), which record downwastage of the Welsh Ice Cap at 19 - 20 ka (≤ 600 m), while ^{14}C ages from proximal Welsh lowlands (15.82 ± 0.39 cal. ka BP; Lowe, 1981; Reimer et al., 2013), show that Alpine-style valley glaciers were present for ~4 ka after initial summit emergence (Hughes et al., 2016). These data also accord with a ^{36}Cl age from ice-sculpted bedrock in the Scafell massif, which indicates substantial downwastage of the Lake District ice cap by 17.3 ± 1.1 ka (< 750 m; Ballantyne et al., 2009). Deglaciation of Carrigshouk at ~16.6 ka marks a shift to topographically confined ice flow, with glaciers sourced from high elevation cirques, and likely reflects a time-progressive response to reduced moisture availability and winter aridity during this interval (Kelly et al., 2010). However, these data indicate that summit ice fields and large valley glaciers persisted in the Wicklows for 4 - 7 ka after ISIS retreat (Smedley et al., 2017b), and reveal similarities in the post-LGM histories of the Wicklow, Welsh (Hughes et al., 2016) and Lake District ice caps (Ballantyne et al., 2009). These data accord with wider evidence for post-LGM disintegration of the BIIS into component ice caps (Clark et al., 2012).

Secondly, the geomorphological record indicates that post-LGM retreat was dynamic, with valley and cirque re-advance moraines deposited during the Oldest Dryas and Younger

Dryas respectively (Fig. 2A). Re-advance of valley glaciers during the interval 15.4 - 16.5 ka was coeval with peak ice rafted debris flux (Bard et al., 2000; Eynaud et al., 2009) and reduced sea surface temperatures (Bard et al., 2000) during Heinrich Stadial 1 (Fig. 2B; HS1) and the re-advance of the Irish Ice Sheet (IIS) and the ISIS during the Killard Point Stadial (~16 - 17.1 ka; McCabe et al., 2007; Clark et al., 2012). The re-advance of glaciers in Ireland during the Oldest Dryas was matched further down the North-East Atlantic margin in Spain (Palacios et al., 2017). These re-advances are linked to North Atlantic climate perturbations (HS1) and likely reflect short-term oscillations of the ice front (≤ 1 ka) during the long-term post-LGM retreat phase (~8 ka). Moreover, these chronological data match recent morphostratigraphic assessments which support a widespread pattern of sustained retreat interrupted by minor glacier readvance (Knight et al., 2017). Retreat from re-advance positions, estimated at 1.82 km ka^{-1} for the Glenmacnass glacier, was synchronous across the Wicklow Mountains, as demonstrated by progressive deglaciation from low to high elevation (Fig. 3A; R^2 = 0.9116; p = 0.045). These data are indicative of climate-controlled retreat with independent outlet glaciers responding synchronously to reduced moisture availability (Kelly et al., 2010), irrespective of contrasting glacier aspects, source areas or glacier extents. Oldest Dryas valley glaciers were extensive (≤ 12.5 km^2), sustained by ice fields and prior to ~16.6 ka, overtopped low-lying summits (~571 m). As a result, the potential for significant redistribution of snow and avalanche material (Ac > Ag) was limited, particularly during periods of winter aridity (Kelly et al., 2010). Therefore, while topography likely influenced the retreat pattern in individual valleys, post-LGM retreat (~15 - 17 ka) was primarily paced by climate.

In contrast, marked asynchroneity in the timing of final YD deglaciation (Fig. 3; 11.4 - 12.3 ka) is unrelated to cirque elevation (Fig. 3A; R^2 < 0.01, p = 0.97), palaeo-ELA (Fig. 3E; R^2 = 0.04, p = 0.81) or site latitude (R^2 = 0.10, p = 0.69). These data suggest that climate was not the dominant control on the timing of final YD deglaciation. Instead, glacier retreat was strongly controlled by local topography and the redistribution of wind-blown snow and avalanche material (Fig. 3B; R^2 > 0.99, p < 0.01). Combined snow and avalanche contributing areas (A_c) range from just 0.119 km^2 at Upper Lough Bray to 1.071 km^2 at Lough Nahanagan. For glaciers with large A_c areas, topography may exert the primary control on glacier formation and survival, and may account for the comparatively late-deglaciation of Lough Nahanagan and Mullaghcleevaun during the early-Holocene. By comparison, glaciers with small A_c areas, where the potential for redistribution of snow and avalanche material is limited, may respond quasi-synchronously to climate warming. For example, the early deglaciation of Upper Lough Bray at 12.31 ± 0.51 ka is coeval with a gradual rise is summer air temperatures after ~12.5 ka (Brooks and Birks, 2000) which was likely sufficient to raise the 'climatic' ELA above cirque elevations (A_c/A_g = 0; Barr et al., 2017) and initiate mass wastage. In contrast, abundant snow redistribution (A_c ≥ 1), conditioned by existing topographic configurations (extensive upland plateaus), was likely sufficient to locally supress the 'local' (non-climatic) ELA and promote glacier survival at other sites. However, the contribution of redistributed snow to glacier accumulation almost certainly diminished throughout the YD as summer air temperatures

increased rapidly towards the onset of the Holocene (Brooks and Birks, 2000), thus limiting snowpack preservation. These data indicate that while regional climate provides the baseline conditions for glacier growth and decay, cirque glacier dynamics may primarily reflect the influence of topography. However, there is a weak correlation between glacier size (A_g) and deglaciation age (Fig. 3C; R^2 = 0.77, p = 0.12), although the size variation between the smallest (ULB; 0.35 km^2) and largest reconstructed glacier (LN: 1.10 km^2) is minimal (~0.75 km^2). As such, significant within-mountain range variation in glacier response times is not anticipated (Raper and Braithwaite, 2009). This may account for the weak correlation between A_c/A_g ratios and deglaciation ages (Fig. 3D; R^2 = 0.58, p = 0.24) although the observable trend demonstrates the probability of early deglaciation for glaciers with small A_c/A_g ratios. Based on this reasoning, we conclude that for small YD glaciers, local topoclimatic controls can be more significant than wider regional climate in determining cirque glacier dynamics, and in particular, the timing of final deglaciation. This result has important implications for palaeoclimate reconstructions based on dating of cirque moraines (e.g. using ^{10}Be), as cirque glacier ELAs are not representative of the regional climate and consequently glaciers dynamics are likely to be decoupled from climatic changes occurring in the North Atlantic region. This phenomenon is observed today in the behaviour of small glaciers in marginal glaciated settings such as the Italian Alps (Colucci, 2016) and other Mediterranean mountains (Hughes, 2018). These data from Ireland also show that the impact of topography on glacier dynamics is most significant when glaciers are small (≤ 1 km^2), resulting in clear asynchroneity in deglaciation (Fig. 3A; R^2 = < 0.01), and provide further evidence that the climatic integrity of cirque glaciers may be limited (Kirkbride and Winkler, 2012). In contrast, large glaciers (~12.5 km^2), with limited potential for snow redistribution, have been shown to respond synchronously to climate forcing (Fig. 3A; R^2 = 0.9116). Modelling studies have shown that topoclimatic variables (solar radiation/snow redistribution) can predict the style of deglaciation (moraine distribution) for small Younger Dryas glaciers (Coleman et al., 2009; Bickerdike et al., 2017). The chronological data presented here provides new evidence that topographic controls not only influence the style of deglaciation, but can determine the timing of final deglaciation, with clear within-mountain range variability.

A further challenge in linking cirque glacier dynamics to climatic fluctuations is the potential impact of moraine stabilisation (Hallet and Putknonen, 1994). This post-depositional process can result in moraine ages (e.g. ^{10}Be) which post-date glacial retreat. A 1-2 ka early stabilization period has been recorded for Alpine moraine sequences in Alaska and the Alps (Briner et al., 2005; Ivy-Ochs et al., 2006, 2008; Dortch et al., 2010a). In these environments, glaciers can produce distinctive asymmetric ice-contact fans that undergo rapid gullying and post-depositional reworking on their ice-proximal slopes (e.g. Hambrey et al., 2012; Lukas et al., 2012). However, these landforms are topographically and sedimentologically distinct from the low-relief, topographically concordant valley and cirque landsystems found in the Wicklow Mountains. Moreover, there has been comparatively little attention to processes of moraine development and deglaciation dynamics in these environments, with analogue

studies predominantly focused on 'hummocky moraine' landsystems (e.g. Benn and Lukas, 2006), and a relative paucity of research into moraine processes in smaller cirque type landsystems, likely under the assumption of rapid stabilisation after deglaciation. Recent work has highlighted the importance of self-censoring in cirque environments due to obliterative overlap (Barr and Lovell, 2014) or ice-cored moraine degradation (Crump et al., 2017; Tonkin et al., 2017), while external-censoring due to slope instability may also provide a control on moraine stabilisation (Barr and Lovell, 2014). As a result, there is considerable uncertainty regarding the robustness of chronological datasets for cirque moraine systems (Kirkbride and Winkler, 2012). To produce better-resolved glacier chronologies, researchers can account for moraine stabilisation through (1) morphostratigraphic comparison of moraine sequences, (2) Gaussian separation of exposure ages (Dortch et al., 2013), (3) assessment against independent geochronological data (e.g. ^{14}C, OSL) and (4) consideration of modern process studies and likely modern analogues for moraine assemblages when assessing site suitability for a give geochronological approach (e.g. Çiner et al. 2015). Based on these criteria, we infer that moraine stabilisation may be a key post-depositional process for the outer moraine at Lough Nahanagan. Firstly, this moraine is degraded (Colhoun and Synge, 1980) and is morphologically distinct from sampled cirque moraines at Mullaghcleevaun, Kelly's Lough and Upper Lough Bray which are tall (> 3 m), matrix-poor, boulder-rich, and feature clearly defined moraine crests (Fig. 4). Secondly, Gaussian separation of SHED data for this site (n = 20) reveals a clear 'two-peak' probability density function (Fig. 2C), with Gaussian ages of 10.93 ± 0.26 ka (n = 9) and 11.38 ± 0.26 ka (n = 9). The youngest age post-dates the YD by ~0.8 ka and is inconsistent with wider evidence for deglaciation of the British Isles by the YD/Holocene transition (MacLeod et al., 2011) although in isolation, this observation is insufficient to reject this age at this stage. In addition, this method highlights clear outlier ages (n = 3; 12.8 - 13.5 ka). These Gaussian ages can be rejected as they are comprised of fewer than 3 ages (c.f. Fig. 3 in Dortch et al., 2013). Finally, independent ^{14}C ages indicate deglaciation during the late YD and early Holocene (11.5 - 11.6 ka; Colhoun and Synge, 1980). In contrast, a single ^{36}Cl age suggests ice free conditions since 17.9 ± 1.0 ka (Bowen et al., 2002), although this age likely reflects prior exposure (*inheritance*) and is rejected from further analysis. Based on these data, we conclude that the older Gaussian age of 11.38 ± 0.26 ka is more representative of final deglaciation as this age is consistent with previous ^{14}C ages and accounts for both the distinctive geomorphological assemblage at this site and the clear 'two-peak' distribution of SHED ages. This conclusion indicates that moraine stabilisation and boulder exhumation may account for the degraded moraine surface and comparatively '*young*' SHED ages. These data provide further evidence that moraine ages are more likely influenced by post-glacial instability than prior exposure (Shanahan & Zreda 2000; Putkonen & Swanson 2003; Zech et al. 2005; Heyman et al. 2011; Applegate et al., 2012). As a result, the dynamics of small cirque glaciers (< 1 km^2), as determined by radiometric methods (^{10}Be), may not only primarily reflect topographic controls, but may be profoundly influenced by post-depositional processes. The post-depositional evolution of YD moraine systems is largely unexplored at

present and a clear co-benefit of the SHED approach is the potential insight into these processes; insight that was not afforded by other geochronological approaches. Future research should carefully consider landform context (Barr and Lovell, 2014) and prioritise sampling of cirque environments where snow and avalanche contributing areas (A_c) are small (Warren, 1991; Mills et al., 2012; Barr and Lovell, 2014), where postglacial erosion is limited and where short transport distances promote the formation of matrix-poor boulder-rich moraines (Fig. 5; Pallàs et al., 2010). In these environments, snow redistribution is limited and moraines are more likely to stabilise rapidly after deglaciation. As such, these glaciers may respond quasi-synchronously to climatic fluctuations and may produce more robust palaeoclimatic reconstructions.

Conclusions

This study provides the first chronological constraints on post-LGM retreat of the Wicklow Ice Cap. 170 SH exposure ages from cirque and valley moraines and from a summit overridden by ice at the LGM demonstrate that significant ice masses persisted in the Wicklows after retreat of the ISIS and were sustained by summit ice-fields until ~16.6 ka. Post-LGM retreat was dynamic, with re-advance moraines deposited during the Oldest Dryas in response to HS1 cooling. However, these events reflect short-term oscillations (≤ 1 ka) of the ice front during the long-term retreat phase (~8 ka), which was driven by reduced moisture availability and winter aridity. This chronology is matched by ^{10}Be and ^{14}C ages from the Welsh Ice Cap, with downwastage during the interval 19-20 ka, while alpine valley glaciers persisted for ~4 ka after initial summit emergence. Retreat from re-advance positions was paced by climate, with time-progressive deglaciation from low to high elevation (R^2 = 0.9116). In contrast, asynchroneity in final Younger Dryas deglaciation is accounted for by local topography and the redistribution of snow and avalanche material. Contrasting synchroneity in the timing of glacial retreat during these periods is conditioned by glacier size, with small YD glaciers (< 1 km^2) highly sensitive to local topographic controls. This result has important implications for palaeoclimate reconstructions based on dating of cirque moraines (e.g. ^{10}Be), as cirque glacier dynamics may be unrelated to climate. This is further complicated by post-depositional processes which can result in ages which post-date retreat. As a result, future palaeoclimate reconstructions should prioritise cirque glaciers where snow and avalanche contributing areas (A_c) are small and where the potential for post-depositional disturbance is limited (matrix-poor, boulder rich moraines).

Acknowledgements

MT is funded by a University of Manchester Presidents Doctoral Scholarship. Fieldwork was funded by the University of Manchester School of Environment, Education and Development

Fieldwork Support Fund. We would like to thank D. Tomkins for fieldwork support and D. Fabel for kindly providing unpublished calibration data for the LLPR.

References

Applegate PJ, Urban NM, Keller K, Lowell T V, Laabs BJC, Kelly MA, Alley RB. 2012. Improved moraine age interpretations through explicit matching of geomorphic process models to cosmogenic nuclide measurements from single landforms. *Quaternary Research* **77**: 293–304.

Balco G, Stone JO, Lifton NA, Dunai TJ. 2008. A complete and easily accessible means of calculating surface exposure ages or erosion rates from ^{10}Be and ^{26}Al measurements. *Quaternary Geochronology* **3**: 174–195.

Ballantyne CK. 2007a. Loch Lomond Stadial glaciers in North Harris, Outer Hebrides, North-West Scotland: glacier reconstruction and palaeoclimatic implications. *Quaternary Science Reviews* **26**: 3134–3149.

Ballantyne CK. 2007b. The Loch Lomond Readvance on north Arran, Scotland: glacier reconstruction and palaeoclimatic implications. *Journal of Quaternary Science* **22**: 343–359.

Ballantyne CK, Mccarroll D, Stone JO. 2006. Vertical dimensions and age of the Wicklow Mountains ice dome, Eastern Ireland, and implications for the extent of the last Irish Ice Sheet. *Quaternary Science Reviews* **25**: 2048–2058.

Ballantyne CK, McCarroll D, Stone JO. 2007. The Donegal ice dome, northwest Ireland: dimensions and chronology. *Journal of Quaternary Science* **22**: 773–783.

Ballantyne CK, Stone JO. 2015. Trimlines, blockfields and the vertical extent of the last ice sheet in southern Ireland. *Boreas* **44**: 277–287.

Ballantyne CK, Stone JO, Fifield LK. 2009. Glaciation and deglaciation of the SW Lake District, England: implications of cosmogenic ^{36}Cl exposure dating. *Proceedings of the Geologists' Association* **120**: 139–144.

Bard E, Rostek F, Turon J louis, Gendreau S. 2000. Hydrological Impact of Heinrich Events in the Subtropical Northeast Atlantic. *Science* **289**: 1321–1324.

Barr ID, Lovell H. 2014. A review of topographic controls on moraine distribution. *Geomorphology* **226**: 44–64.

Barr ID, Roberson S, Flood R, Dortch J. 2017. Younger Dryas glaciers and climate in the Mourne Mountains, Northern Ireland. *Journal of Quaternary Science* **32**: 104–115.

Benn DI, Lukas S. 2006. Younger Dryas glacial landsystems in North West Scotland: an assessment of modern analogues and palaeoclimatic implications. *Quaternary Science Reviews* **25**: 2390–2408.

Bickerdike HL, Ó Cofaigh C, Evans DJA, Stokes CR. 2017. Glacial landsystems, retreat dynamics and controls on Loch Lomond Stadial (Younger Dryas) glaciation in Britain. *Boreas*.

Birks HJB. 2001. Chironomid-inferred Late-glacial air temperatures at Whitrig Bog, southeast Scotland. *Journal of Quaternary Science* **15**: 759–764.

Bowen DQ, Phillips FM, McCabe AM, Knutz PC, Sykes GA. 2002. New data for the Last Glacial Maximum in Great Britain and

Ireland. *Quaternary Science Reviews* **21**: 89–101.

Briner JP, Kaufman DS, Manley WF, Finkel RC, Caffee MW. 2005. Cosmogenic exposure dating of late Pleistocene moraine stabilization in Alaska. *GSA Bulletin* **117**: 1108–1120.

Chiverrell RC, Thrasher IANM, Thomas GSP, Lang A, Scourse JD, Van Landeghem KJJ, McCarroll D, Clark CD, Ó Cofaigh C, Evans DJA, Ballantyne CK. 2013. Bayesian modelling the retreat of the Irish Sea Ice Stream. *Journal of Quaternary Science* **28**: 200–209.

Çiner A, Sarıkaya MA, Yıldırım C. 2015. Late Pleistocene piedmont glaciations in the Eastern Mediterranean; insights from cosmogenic ^{36}Cl dating of hummocky moraines in southern Turkey. *Quaternary Science Reviews* **116**: 44–56.

Clark J, Cabe AMMC, Schnabel C, Clark PU, Freeman S, Maden C, Xu S. 2009. ^{10}Be chronology of the last deglaciation of County Donegal, northwestern Ireland. *Boreas* **38**: 111–118.

Clark CD, Ely JC, Greenwood SL, Hughes ALC, Meehan R, Barr ID, Bateman MD, Bradwell T, Doole J, Evans DJA, Jordan CJ, Monteys X, Pellicer XM, Sheehy M. 2017. BRITICE Glacial Map, version 2: a map and GIS database of glacial landforms of the last British-Irish Ice Sheet. *Boreas*.

Clark CD, Hughes ALC, Greenwood SL, Jordan C, Sejrup HP. 2012. Pattern and timing of retreat of the last British-Irish Ice Sheet. *Quaternary Science Reviews* **44**: 112–146.

Coleman CG, Carr SJ, Parker AG. 2009. Modelling topoclimatic controls on palaeoglaciers: implications for inferring palaeoclimate from geomorphic evidence. *Quaternary Science Reviews* **28**: 249–259.

Colhoun EA, Synge MF. 1980. The Cirque Moraines at Lough Nahanagan, County Wicklow, Ireland. *Proceedings of the Royal Irish Academy. Section B: Biological, Geological, and Chemical Science* **80**: 25–45.

Colucci RR. 2016. Geomorphic influence on small glacier response to post-Little Ice Age climate warming: Julian Alps, Europe. *Earth Surface Processes and Landforms* **41**: 1227–1240.

Crump SE, Anderson LS, Miller GH, Anderson RS. 2017. Interpreting exposure ages from ice-cored moraines: a Neoglacial case study on Baffin Island, Arctic Canada. *Journal of Quaternary Science* **32**: 1049–1062.

Demirdag S, Yavuz H, Altindag R. 2009. The effect of sample size on Schmidt rebound hardness value of rocks. *International Journal of Rock Mechanics and Mining Sciences* **46**: 725–730.

Dortch JM, Hughes PD, Tomkins MD. 2016. Schmidt hammer exposure dating (SHED): Calibration boulder of Tomkins et al. (2016). *Quaternary Geochronology* **35**: 67–68.

Dortch JM, Owen LA, Caffee MW. 2013. Timing and climatic drivers for glaciation across semi-arid western Himalayan-Tibetan orogen. *Quaternary Science Reviews* **78**: 188–208.

Dortch JM, Owen LA, Caffee MW, Brease P. 2010. Late Quaternary glaciation and equilibrium line altitude variations of the McKinley River region, central Alaska Range. *Boreas* **39**: 233–246.

Eynaud F, de Abreu L, Voelker A, Schönfeld J, Salgueiro E, Turon JL, Penaud A, Toucanne S, Naughton F, Sánchez Goñi

MF, Malaizé B, Cacho I. 2009. Position of the Polar Front along the western Iberian margin during key cold episodes of the last 45 ka. *Geochemistry, Geophysics, Geosystems* **10**.

Fabel D, Ballantyne CK, Xu S. 2012. Trimlines, blockfields, mountain-top erratics and the vertical dimensions of the last British- Irish Ice Sheet in NW Scotland. *Quaternary Science Reviews* **55**: 91–102.

Glasser NF, Hughes PD, Fenton C, Schnabel C, Rother H. 2012. ^{10}Be and ^{26}Al exposure-age dating of bedrock surfaces on the Aran ridge, Wales: evidence for a thick Welsh Ice Cap at the Last Glacial Maximum. *Journal of Quaternary Science* **27**: 97–104.

Hallet B, Putkonen J. 2017. Surface Dating of Dynamic Landforms: Young Boulders on Aging Moraines. *Science* **265**: 937–940.

Hambrey MJ, Quincey DJ, Glasser NF, Reynolds JM, Richardson SJ, Clemmens S. 2008. Sedimentological, geomorphological and dynamic context of debris-mantled glaciers, Mount Everest (Sagarmatha) region, Nepal. *Quaternary Science Reviews* **27**: 2361–2389.

Heyman J, Stroeven AP, Harbor JM, Caffee MW. 2010. Too young or too old: Evaluating cosmogenic exposure dating based on an analysis of compiled boulder exposure ages. *Earth and Planetary Science Letters* **302**: 71–80.

Hughes PD. 2018. Little Ice Age glaciers and climate in the Mediterranean mountains: A new analysis. *Cuadernos de Investigación Geográfica* **44**.

Hughes PD, Braithwaite RJ. 2008. Application of a degree-day model to reconstruct Pleistocene glacial climates. *Quaternary Research* **69**: 110–116.

Hughes PD, Gibbard PL. 2015. A stratigraphical basis for the Last Glacial Maximum (LGM). *Quaternary International* **383**: 174–185.

Hughes PD, Glasser NF, Fink D. 2016. Rapid thinning of the Welsh Ice Cap at 20-19 ka based on ^{10}Be ages. *Quaternary Research* **85**: 107–117.

Ivy-Ochs S, Kerschner H, Reuther A, Maisch M, Sailer R, Kubik PW, Synal HA, Schlüchter C. 2006. The timing of glacier advances in the northern European Alps based on surface exposure dating with cosmogenic ^{10}Be, ^{26}Al, ^{36}Cl, and ^{21}Ne. In: Siame LL,, In: Bourlès DL,, In: Brown ET, eds. *In Situ–Produced Cosmogenic Nuclides and Quantifi cation of Geological Processes: Geological Society of America Special Paper* **415**. Geological Society of America, 43–60.

Ivy-Ochs S, Kerschner H, Reuther A, Preusser F, Heine K, Maisch MAX, Kubik PW, Schlüchter C. 2008. Chronology of the last glacial cycle in the European Alps. *Journal of Quaternary Science* **23**: 559–573.

Kelly A, Charman DJ, Newnham RM. 2010. A Last Glacial Maximum pollen record from Bodmin Moor showing a possible cryptic northern refugium in southwest England. *Journal of Quaternary Science* **25**: 296–308.

Kern Z, László P. 2010. Size specific steady-state accumulation-area ratio: an improvement for equilibrium-line estimation of small palaeoglaciers. *Quaternary Science Reviews* **29**: 2781–2787.

Kirkbride MP, Winkler S. 2012. Correlation of Late Quaternary moraines: impact of climate variability, glacier response, and chronological resolution. *Quaternary Science Reviews* **46**: 1–29.

Knight L, Boston C, Lovell H, Pepin N. 2017.

Last Glacial-Interglacial Transition ice dynamics in the Wicklow Mountains, Ireland. *Geophysical Research Abstracts* **19**.

Lal D. 1991. Cosmic ray labeling of erosion surfaces: in situ nuclide production rates and erosion models. *Earth and Planetary Science Letters* **104**: 424–439.

Lloyd JM, Zong Y, Fish P, Innes JB. 2013. Holocene and Lateglacial relative sea-level change in north-west England: implications for glacial isostatic adjustment models. *Journal of Quaternary Science* **28**: 59–70.

Lowe S. 1981. Radiocarbon dating and stratigraphic resolution in Welsh lateglacial chronology. *Nature* **293**: 210–212.

Lukas S, Graf A, Coray S, Schlüchter C. 2012. Genesis , stability and preservation potential of large lateral moraines of Alpine valley glaciers e towards a unifying theory based on Findelengletscher , Switzerland. *Quaternary Science Reviews* **38**: 27–48.

Macleod A, Palmer A, Lowe J, Rose J, Bryant C, Merritt J. 2011. Timing of glacier response to Younger Dryas climatic cooling in Scotland. *Global and Planetary Change* **79**: 264–274.

Matthews JA, Owen G. 2008. Endolithic lichens, rapid biological weathering and Schmidt Hammer R-Values on recently exposed rock surfaces: Storbreen glacier foreland, Jotunheimen, Norway. *Geografiska Annaler, Series A: Physical Geography* **90**: 287–297.

McCabe AM, Clark PU, Clark J, Dunlop P. 2007. Radiocarbon constraints on readvances of the British-Irish Ice Sheet in the northern Irish Sea Basin during the last deglaciation. *Quaternary Science Reviews* **26**: 1204–1211.

McCarroll D, Stone JO, Ballantyne CK, Scourse JD, Fifield LK, Evans DJA, Hiemstra JF. 2010. Exposure-age constraints on the extent , timing and rate of retreat of the last Irish Sea ice stream. *Quaternary Science Reviews* **29**: 1844–1852.

Mills SC, Grab SW, Rea BR, Carr SJ, Farrow A. 2012. Shifting westerlies and precipitation patterns during the Late Pleistocene in southern Africa determined using glacier reconstruction and mass balance modelling. *Quaternary Science Reviews* **55**: 145–159.

Mitchell WA. 1996. Significance of snowblow in the generation of Loch Lomond Stadial (Younger Dryas) glaciers in the western Pennines, northern England. *Journal of Quaternary Science* **11**: 233–248.

Murari MK, Owen LA, Dortch JM, Caffee MW, Dietsch C, Fuchs M, Haneberg WC, Sharma MC, Townsend-Small A. 2014. Timing and climatic drivers for glaciation across monsoon-influenced regions of the Himalayan-Tibetan orogen. *Quaternary Science Reviews* **88**: 159–182.

Niedzielski T, Migoń P, Placek A. 2009. A minimum sample size required from Schmidt hammer measurements. *Earth Surface Processes and Landforms* **34**: 1713–1725.

Ohmura A, Kasser P, Funk M. 1992. Climate at the equilibrium line of glaciers. *Journal of Glaciology* **38**: 397–411.

Palacios D, García-Ruiz JM, Andrés N, Schimmelpfennig I, Campos N, Léanni L, Team A. 2017. Deglaciation in the central Pyrenees during the Pleistocene e Holocene transition: Timing and geomorphological significance. *Quaternary Science Reviews* **162**: 111–127.

Pallàs R, Rodés Á, Braucher R, Bourlès D, Delmas M, Calvet M, Gunnell Y. 2010. Small, isolated glacial catchments as priority targets for cosmogenic surface exposure dating of Pleistocene climate fluctuations, southeastern Pyrenees. *Geology* **38**: 891–894.

Pellitero R, Rea BR, Spagnolo M, Bakke J, Hughes P, Ivy-Ochs S, Lukas S, Ribolini A. 2015. A GIS tool for automatic calculation of glacier equilibrium-line altitudes. *Computers and Geosciences* **82**: 55–62.

Pellitero R, Rea BR, Spagnolo M, Bakke J, Ivy-Ochs S, Frew CR, Hughes P, Ribolini A, Lukas S, Renssen H. 2016. GlaRe, a GIS tool to reconstruct the 3D surface of palaeoglaciers. *Computers and Geosciences* **94**: 77–85.

Putkonen J, Swanson T. 2003. Accuracy of cosmogenic ages for moraines. *Quaternary Research* **59**: 255–261.

Rea BR. 2009. Defining modern day Area-Altitude Balance Ratios (AABRs) and their use in glacier-climate reconstructions. *Quaternary Science Reviews* **28**: 237–248.

Reimer PJ, Bard E, Bayliss A, Beck JW, Blackwell PG, Bronk Ramsey C, Buck CE, Cheng H, Edwards RL, Friedrich M, Grootes PM, Guilderson TP, Haflidason H, Hajdas I, Hatté C, Heaton TJ, Hoffman DL, Hogg AG, Hughen KA, Kaiser KF, Kromer B, Manning SW, Niu M, Reimer RW, Richards DA, Scott EM, Southon JR, Staff RA, Turney CSM, van der Plicht J. 2013. Intcal13 and marine13 radiocarbon age calibration curves 0 – 50,000 years cal BP. *Radiocarbon* **55**: 1869–1887.

Shanahan TM, Zreda M. 2000. Chronology of Quaternary glaciations in East Africa. *Earth and Planetary Science Letters* **177**: 23–42.

Smedley RK, Chiverrell RC, Ballantyne CK, Burke MJ, Clark CD, Duller GAT, Fabel D, McCarroll D, Scourse JD, Small D, Thomas GSP. 2017a. Internal dynamics condition centennial-scale oscillations in marine-based ice-stream retreat. *Geology* **45**: 787–790.

Smedley RK, Scourse JD, Small D, Hiemstra JF, Duller GAT, Bateman MD, Burke MJ, Chiverrell RC, Clark CD, Davies SM, Fabel D, Gheorghiu DM, McCarroll D, Medialdea A, Xu S. 2017b. New age constraints for the limit of the British-Irish Ice Sheet on the Isles of Scilly. *Journal of Quaternary Science* **32**: 48–62.

Stone JO. 2000. Air pressure and cosmogenic isotope production. *Journal of Geophysical Research* **105**: 23753–23759.

Sumner P, Nel W. 2002. The effect of rock moisture on Schmidt hammer rebound: Tests on rock samples from Marion Island and South Africa. *Earth Surface Processes and Landforms* **27**: 1137–1142.

Tomkins MD, Dortch JM, Hughes PD. 2016. Schmidt Hammer exposure dating (SHED): Establishment and implications for the retreat of the last British Ice Sheet. *Quaternary Geochronology* **33**: 46–60.

Tomkins MD, Huck JJ, Dortch JM, Hughes PD, Kirkbride MJ, Barr IB. 2017. Schmidt Hammer exposure dating (SHED): Calibration procedures, new exposure age data and an online calculator. *Quaternary Geochronology*. Accepted Manuscript.

Tonkin TN, Midgley NG, Graham DJ, Labadz JC. 2017. Internal structure and significance of ice-marginal moraine in the Kebnekaise Mountains, northern Sweden. *Boreas* **46**: 199–211.

Warren CR. 1991. Terminal environment, topographic control and fluctuations of

West Greenland glaciers. *Boreas* **20**: 1–15.

Williams RBG, Robinson DA. 1983. The effect of surface texture on the determination of the surface hardness of rock using the Schmidt Hammer. *Earth Surface Processes and Landforms* **8**: 289–292.

Wilson P, Schnabel C, Wilcken KM, Vincent PJ. 2013. Surface exposure dating (^{36}Cl and ^{10}Be) of post-Last Glacial Maximum valley moraines, Lake District, northwest England: some issues and implications. *Journal of Quaternary Science* **28**: 379–390.

Zech R, Glaser B, Sosin P, Kubik PW, Zech W. 2005. Evidence for long-lasting landform surface instability on hummocky moraines in the Pamir Mountains (Tajikistan) from ^{10}Be surface exposure dating. *Earth and Planetary Science Letters* **237**: 453–461.

Figure Captions

Figure 1. Generalised geomorphological map of the Wicklow Mountains. Moraines modified after Clark et al. (2017). ^{10}Be ages recalibrated from Ballantyne et al. (2006) using the online calculators formerly known as the CRONUS-Earth online calculator (Wrapper script 2.3, Main calculator 2.1, constants 2.3, muons 1.1; Balco et al., 2008) based on the Loch Lomond Production Rate (Fabel et al., 2012), the time-independent Lm scaling (Lal, 1991; Stone 2000) and assuming 0 mm ka^{-1} erosion. Ca: Camenabologue; Dj: Djouce Mountain; Ka: Kanturk; Ki: Kippure; Lq: Lugnaquillia; Mu: Mullaghcleevaun; Sc: Scarr; Tg: Tonelagee. Map projection: UTM WGS 1984.

Figure 2. Gaussian ages related to deglaciation of the Wicklow Mountains. A: The NGRIP Oxygen Isotope Curve (Rasmussen et al., 2014) plotted against 1σ age boundaries for sampled cirque and valley sites. The Younger Dryas (YD) and Oldest Dryas (OD) periods are

marked. B: Ice rafted debris and sea surface temperature records from cores SUBI-18 (Bard et al., 2000) and MD95-2039 (Eynaud et al., 2009) in the North Atlantic. C: Gaussian models for sampled cirque and valley sites. For each site, the highest probability Gaussian is considered the most likely timing of deglaciation as all ages are younger than the Last Glacial Maximum (Dortch et al., 2013). At Lough Nahanagan, the oldest peak with more than 3 ages is selected (c.f. Dortch et al., 2013) as this moraine is degraded and morphologically distinct from other sampled cirque moraines (MC, KL, ULB). Moreover, this estimates matches previous ^{14}C ages (Colhoun and Synge, 1980).

Figure 3. Topographic and climatic controls on the timing of cirque deglaciation in the Wicklow Mountains. A: Site Elevation; B: Snow contributing area (A_c); C: Glacier area (A_g); D: A_c/A_g ratio; E: ELA; F: ELAs and A_c/A_g ratio plots. These data show that for large valley glaciers, retreat is paced by climate with progressive deglaciation from low to high elevation (A). In contrast, marked asynchroneity in the timing of cirque deglaciation (A) is strongly controlled by snow redistribution (B). This asynchroneity is weakly correlated with glacier size (C) and A_c/A_g ratios (D) and is unrelated to ELA (E).

Figure 4. Sampled cirque moraines at Lough Nahanagan (A), Mullaghcleevaun (B), Kelly's Lough (C) and Upper Lough Bray (D). The outer cirque moraine at Lough Nahanagan is degraded (Colhoun and Synge, 1980) and is morphologically distinct from other cirque moraines which are sharp crested, boulder-rich and matrix-poor.

Figure 5. Matrix-poor, boulder-rich moraine at Mullaghcleevaun which likely stabilised rapidly after deglaciation.

Tables

Table 1. Gaussian ages for cirque, valley and summit sites from the Wicklow Mountains.

Group	Site Name	Site Code	Site Elevation (m)	Site Latitude (°)	Deglaciation Age (ka)	±	Glacier Area (A_g km^2)
Cirque	Lough Nahanagan	LN	443	53.034	11.38	0.26	1.10
	Mullaghcleevaun	MC	571	53.089	11.40	0.13	0.61
	Kelly's Lough	KL	585	52.960	12.00	0.44	0.38
	Upper Lough Bray	ULB	466	53.178	12.31	0.51	0.35
Valley	Lough Brook	LB	393	53.070	15.41	0.30	7.63
	Carrawaystick Brook	CB	421	52.964	15.48	0.35	1.83
	Upper Glendasan	UGD	332	53.030	16.21	0.60	4.96
	Glenmacnass Waterfall	GW	268	53.062	16.46	0.58	12.46
Summit	Carrigshouk	CG	571	53.086	16.64	0.82	-

Table 2. Snow contributing areas (A_c), glacier areas (A_g) and ELAs for cirque moraines.

Site Code	Deglaciation Age (ka)	±	Snow Contributing Area (A_c km^2) [a]	Glacier Area (A_g km^2)	A_c / A_g Ratio	ELA [b]
LN	11.38	0.26	1.07	1.10	0.97	513
MC	11.40	0.13	0.99	0.61	1.62	561
KL	12.00	0.44	0.42	0.38	1.10	648
ULB	12.31	0.51	0.12	0.35	0.34	519

[a] Area within the glacier drainage basin within the 210 – 300° quadrant + all other slopes which overlook the glacier (Gradients > 25°), [b] AABR = 1.9 ± 0.81 (Rea, 2009)

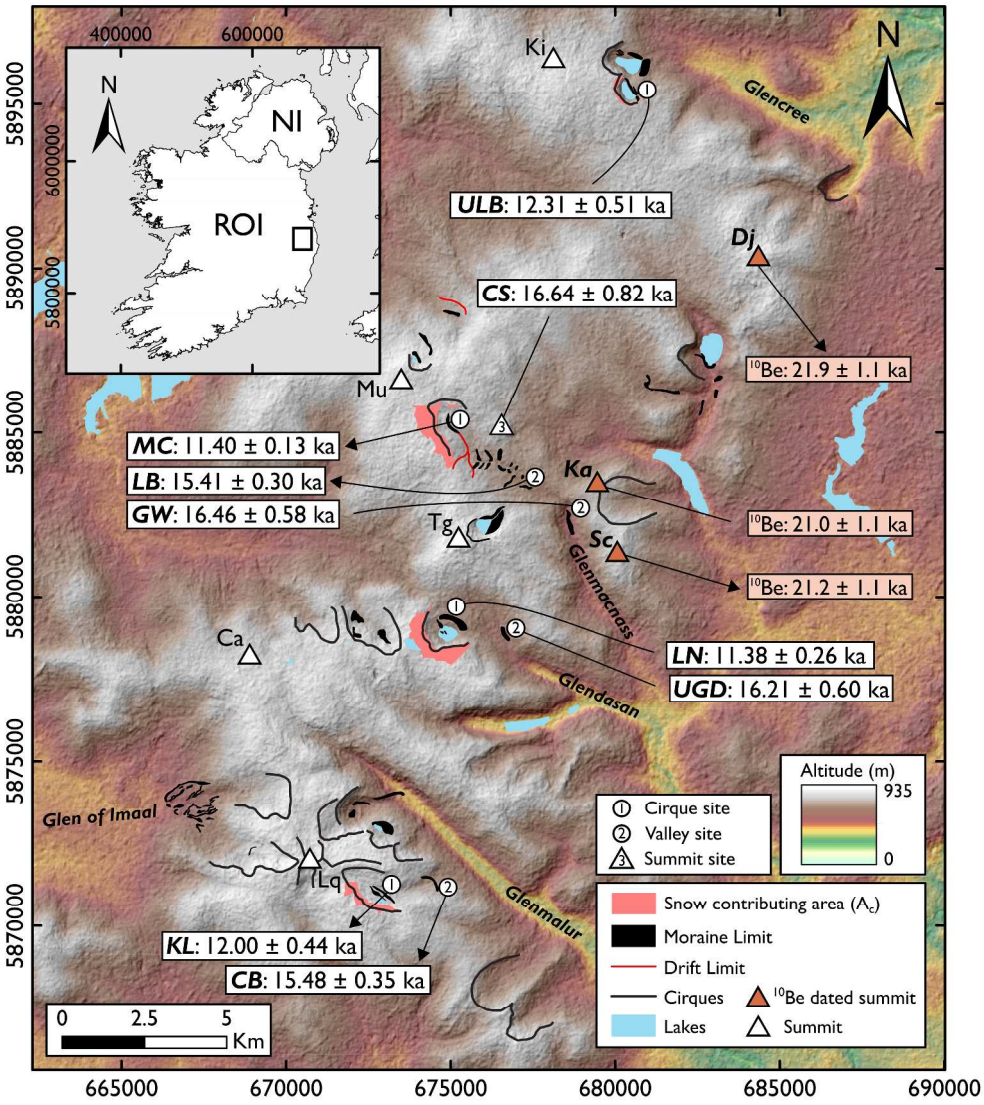

Figure 1. Generalised geomorphological map of the Wicklow Mountains. Moraines modified after Clark et al. (2017). 10Be ages recalibrated from Ballantyne et al. (2006) using the online calculators formerly known as the CRONUS-Earth online calculator (Wrapper script 2.3, Main calculator 2.1, constants 2.3, muons 1.1; Balco et al., 2008) based on the Loch Lomond Production Rate (Fabel et al., 2012), the time-independent Lm scaling (Lal, 1991; Stone 2000) and assuming 0 mm ka-1 erosion. Ca: Camenabologue; Dj: Djouce Mountain; Ka: Kanturk; Ki: Kippure; Lq: Lugnaquillia; Mu: Mullaghcleevaun; Sc: Scarr; Tg: Tonelagee. Map projection: UTM WGS 1984.

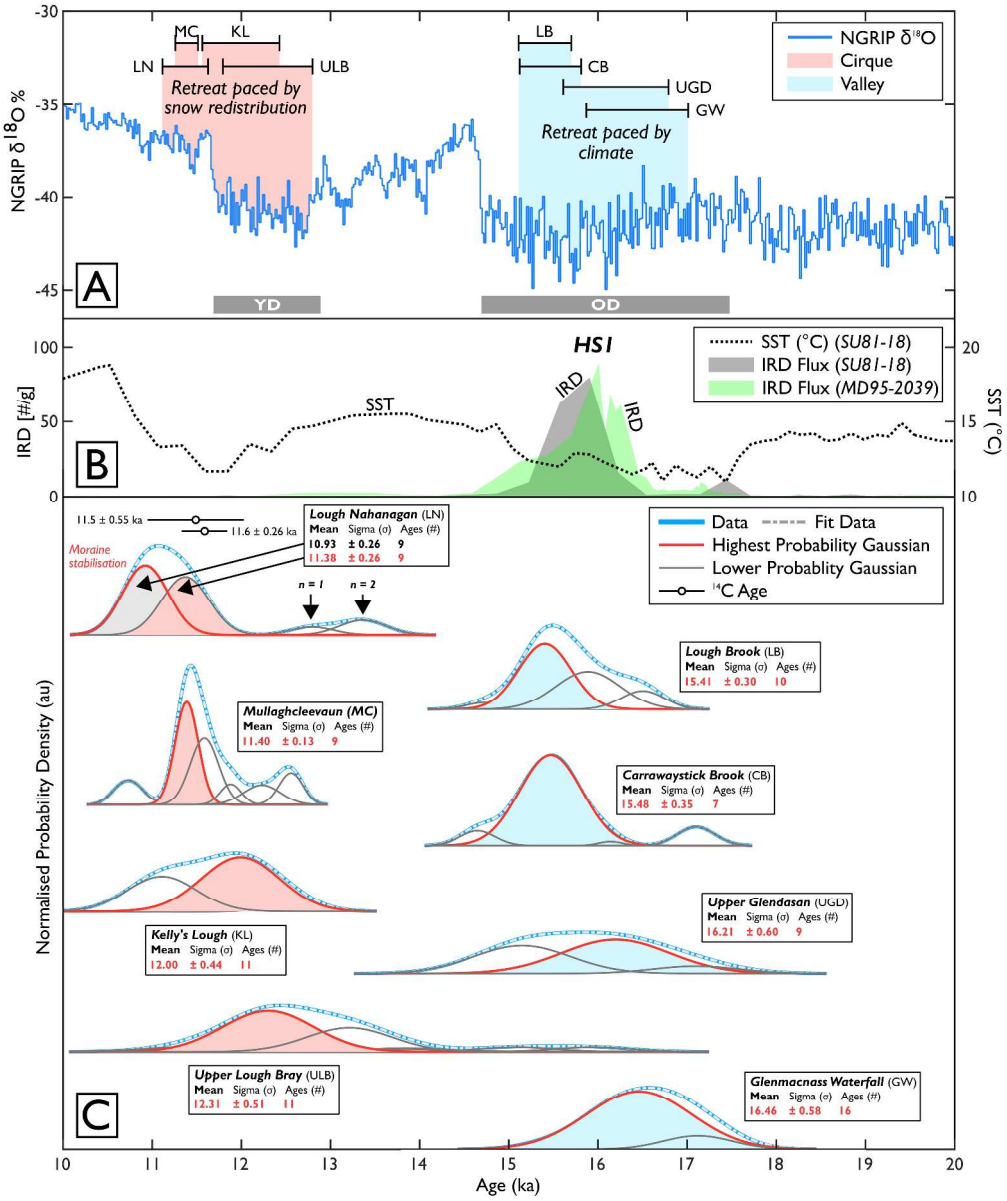

Figure 2. Gaussian ages related to deglaciation of the Wicklow Mountains. A: The NGRIP Oxygen Isotope Curve (Rasmussen et al., 2014) plotted against 1σ age boundaries for sampled cirque and valley sites. The Younger Dryas (YD) and Oldest Dryas (OD) periods are marked. B: Ice rafted debris and sea surface temperature records from cores SUBI-18 (Bard et al., 2000) and MD95-2039 (Eynaud et al., 2009) in the North Atlantic. C: Gaussian models for sampled cirque and valley sites. For each site, the highest probability Gaussian is considered the most likely timing of deglaciation as all ages are younger than the Last Glacial Maximum (Dortch et al., 2013). At Lough Nahanagan, the oldest peak with more than 3 ages is selected (c.f. Dortch et al., 2013) as this moraine is degraded and morphologically distinct from other sampled cirque moraines (MC, KL, ULB). Moreover, this estimates matches previous 14C ages (Colhoun and Synge, 1980).

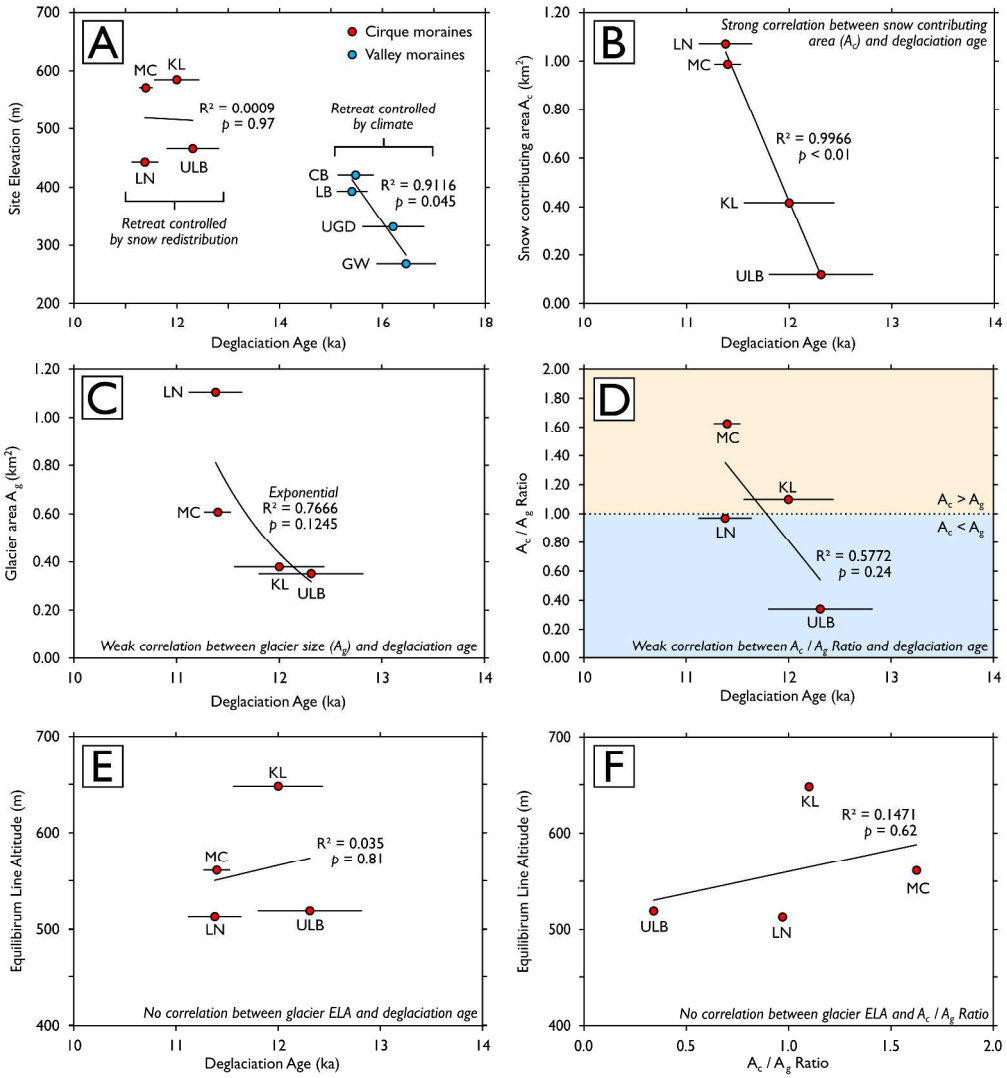

Figure 3. Topographic and climatic controls on the timing of cirque deglaciation in the Wicklow Mountains. A: Site Elevation; B: Snow contributing area (Ac); C: Glacier area (Ag); D: Ac/Ag ratio; E: ELA; F: ELAs and Ac/Ag ratio plots. These data show that for large valley glaciers, retreat is paced by climate with progressive deglaciation from low to high elevation (A). In contrast, marked asynchroneity in the timing of cirque deglaciation (A) is strongly controlled by snow redistribution (B). This asynchroneity is weakly correlated with glacier size (C) and Ac/Ag ratios (D) and is unrelated to ELA (E).

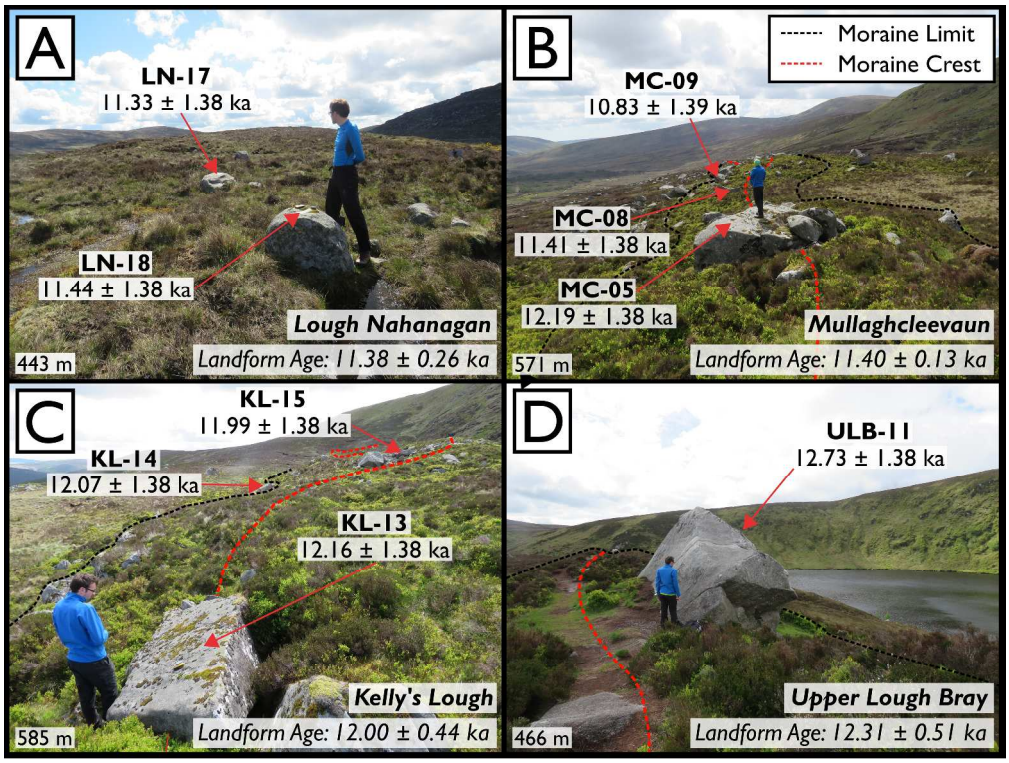

Figure 4. Sampled cirque moraines at Lough Nahanagan (A), Mullaghcleevaun (B), Kelly's Lough (C) and Upper Lough Bray (D). The outer cirque moraine at Lough Nahanagan is degraded (Colhoun and Synge, 1980) and is morphologically distinct from other cirque moraines which are sharp crested, boulder-rich and matrix-poor.

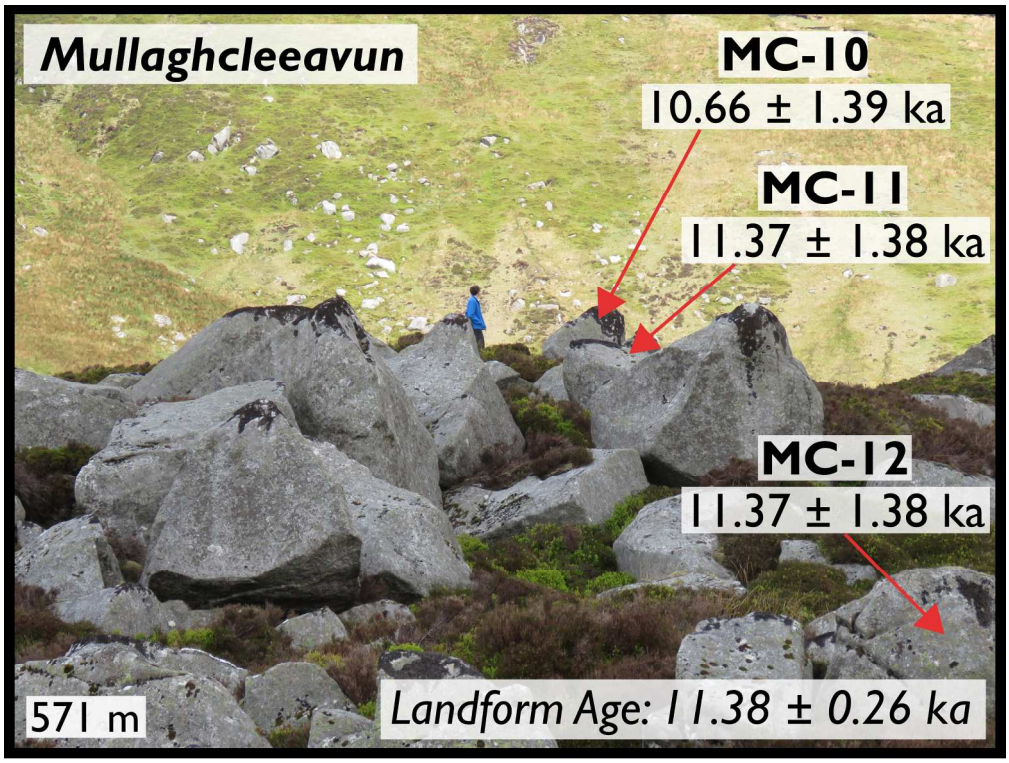

Figure 5. Matrix-poor, boulder-rich moraine at Mullaghcleevaun which likely stabilised rapidly after deglaciation.

Group	Site Code	Sample Name	Latitude (°)	Longitude (°)	Elevation (m)	Type	Mean R-value	SEM [a]	Age (ka)	1σ
Cirque	LN	LN-01	53.03338	-6.3854	445	Boulder	46.10	0.94	11.535	1.382
Cirque	LN	LN-02	53.03352	-6.3858	447	Boulder	46.63	0.92	11.233	1.383
Cirque	LN	LN-03	53.03358	-6.38594	446	Boulder	46.24	0.81	11.46	1.382
Cirque	LN	LN-04	53.03383	-6.3859	446	Boulder	46.91	0.91	11.074	1.384
Cirque	LN	LN-05	53.03407	-6.38591	446	Boulder	47.28	0.98	10.852	1.385
Cirque	LN	LN-06	53.03402	-6.38659	447	Boulder	47.05	1.04	10.971	1.384
Cirque	LN	LN-07	53.03372	-6.3867	447	Boulder	46.42	0.91	11.322	1.383
Cirque	LN	LN-08	53.03381	-6.38705	447	Boulder	42.96	0.64	13.281	1.378
Cirque	LN	LN-09	53.03405	-6.38726	445	Boulder	47.16	0.82	10.892	1.384
Cirque	LN	LN-10	53.03421	-6.38778	444	Boulder	42.63	0.55	13.466	1.377
Cirque	LN	LN-11	53.03463	-6.38824	443	Boulder	46.54	0.87	11.252	1.383
Cirque	LN	LN-12	53.03461	-6.38828	442	Boulder	47.31	0.95	10.816	1.385
Cirque	LN	LN-13	53.03452	-6.38849	443	Boulder	46.18	1.03	11.46	1.382
Cirque	LN	LN-14	53.03478	-6.38881	440	Boulder	47.09	1.05	10.949	1.384
Cirque	LN	LN-15	53.03468	-6.38892	440	Boulder	47.09	0.99	10.949	1.384
Cirque	LN	LN-16	53.03476	-6.39012	439	Boulder	47.23	1.10	10.873	1.384
Cirque	LN	LN-17	53.03477	-6.39019	439	Boulder	46.43	0.94	11.327	1.383
Cirque	LN	LN-18	53.03462	-6.39077	439	Boulder	46.23	0.82	11.441	1.382
Cirque	LN	LN-19	53.03465	-6.39129	438	Boulder	47.01	0.91	11.005	1.384
Cirque	LN	LN-20	53.03481	-6.39209	437	Boulder	43.84	0.82	12.804	1.379
Cirque	MC	MC-01	53.08932	-6.38822	586	Boulder	45.89	0.85	11.636	1.382
Cirque	MC	MC-02	53.08923	-6.38826	586	Boulder	45.50	0.79	11.855	1.381
Cirque	MC	MC-03	53.08913	-6.38826	587	Boulder	46.20	0.76	11.458	1.382
Cirque	MC	MC-04	53.08889	-6.38819	586	Boulder	44.51	0.79	12.414	1.38
Cirque	MC	MC-05	53.08873	-6.38812	583	Boulder	44.92	0.68	12.188	1.38
Cirque	MC	MC-06	53.08862	-6.38807	580	Boulder	46.21	0.91	11.452	1.382
Cirque	MC	MC-07	53.08856	-6.38811	578	Boulder	44.19	0.83	12.599	1.379
Cirque	MC	MC-08	53.08836	-6.38785	575	Boulder	46.28	0.87	11.412	1.383

Cirque	MC	MC-09	53.08817	-6.38766	575	Boulder	47.32	0.90	10.828	1.385
Cirque	MC	MC-10	53.08792	-6.38769	575	Boulder	47.62	0.98	10.657	1.385
Cirque	MC	MC-11	53.08784	-6.38766	575	Boulder	46.36	0.77	11.367	1.383
Cirque	MC	MC-12	53.08763	-6.38737	569	Boulder	46.37	1.09	11.371	1.383
Cirque	MC	MC-13	53.08737	-6.38723	568	Boulder	45.41	0.96	11.914	1.381
Cirque	MC	MC-14	53.08703	-6.38712	568	Boulder	46.28	0.94	11.418	1.382
Cirque	MC	MC-15	53.08699	-6.38697	568	Boulder	46.12	0.97	11.513	1.382
Cirque	MC	MC-16	53.08677	-6.38674	566	Boulder	45.85	1.04	11.655	1.382
Cirque	MC	MC-17	53.08662	-6.38667	564	Boulder	46.42	0.80	11.341	1.383
Cirque	MC	MC-18	53.0861	-6.3857	552	Boulder	46.26	0.87	11.429	1.382
Cirque	MC	MC-19	53.0858	-6.38509	543	Boulder	44.24	0.80	12.571	1.379
Cirque	MC	MC-20	53.08559	-6.38516	542	Boulder	45.90	0.85	11.63	1.382
Cirque	KL	KL-01	52.96091	-6.42741	589	Boulder	47.09	0.69	10.964	1.384
Cirque	KL	KL-02	52.9606	-6.42686	586	Boulder	44.40	0.72	12.491	1.379
Cirque	KL	KL-03	52.96059	-6.42689	585	Boulder	45.40	0.89	11.918	1.381
Cirque	KL	KL-04	52.96058	-6.42695	585	Boulder	45.01	0.59	12.151	1.38
Cirque	KL	KL-05	52.96054	-6.42688	585	Boulder	46.57	0.85	11.252	1.383
Cirque	KL	KL-06	52.96045	-6.42687	585	Boulder	45.31	0.85	11.961	1.381
Cirque	KL	KL-07	52.96037	-6.42682	585	Boulder	46.28	0.66	11.414	1.382
Cirque	KL	KL-08	52.96032	-6.42669	585	Boulder	47.08	0.58	10.962	1.384
Cirque	KL	KL-09	52.96022	-6.42657	585	Boulder	46.59	0.88	11.24	1.383
Cirque	KL	KL-10	52.96015	-6.42655	585	Boulder	44.40	0.83	12.472	1.379
Cirque	KL	KL-11	52.96006	-6.42634	585	Boulder	45.67	0.81	11.749	1.381
Cirque	KL	KL-12	52.9599	-6.42618	585	Boulder	44.57	0.81	12.368	1.38
Cirque	KL	KL-13	52.95984	-6.42605	584	Boulder	44.94	0.81	12.162	1.38
Cirque	KL	KL-14	52.95965	-6.42554	582	Boulder	45.11	0.92	12.067	1.38
Cirque	KL	KL-15	52.95945	-6.42557	586	Boulder	45.25	0.97	11.99	1.381
Cirque	KL	KL-16	52.95947	-6.42537	585	Boulder	47.25	0.99	10.854	1.385
Cirque	KL	KL-17	52.95913	-6.42493	586	Boulder	45.56	0.89	11.819	1.381
Cirque	KL	KL-18	52.95903	-6.42483	586	Boulder	46.69	0.62	11.176	1.383
Cirque	KL	KL-19	52.95883	-6.42416	583	Boulder	45.60	0.74	11.8	1.381
Cirque	KL	KL-20	52.95849	-6.42373	583	Boulder	46.30	0.59	11.403	1.383
Cirque	ULB	ULB-01	53.18062	-6.30129	464	Boulder	44.30	1.00	12.544	1.379

Cirque	ULB	ULB-02	53.18063	-6.30117	463	Boulder	45.17	1.01	12.043	1.381
Cirque	ULB	ULB-03	53.18056	-6.30117	462	Boulder	44.44	1.27	12.459	1.379
Cirque	ULB	ULB-04	53.18044	-6.30134	462	Boulder	44.68	1.40	12.327	1.38
Cirque	ULB	ULB-05	53.18032	-6.30136	462	Boulder	46.33	1.25	11.38	1.383
Cirque	ULB	ULB-06	53.1804	-6.30112	462	Boulder	44.65	1.14	12.334	1.38
Cirque	ULB	ULB-07	53.18048	-6.30083	462	Boulder	45.06	1.24	12.109	1.38
Cirque	ULB	ULB-08	53.18055	-6.30071	462	Boulder	44.73	1.39	12.294	1.38
Cirque	ULB	ULB-09	53.18025	-6.30063	466	Boulder	43.29	1.40	13.116	1.378
Cirque	ULB	ULB-10	53.18022	-6.30049	466	Boulder	44.84	1.08	12.234	1.38
Cirque	ULB	ULB-11	53.17784	-6.29847	471	Boulder	43.97	1.05	12.728	1.379
Cirque	ULB	ULB-12	53.17786	-6.29841	471	Boulder	42.06	0.96	13.813	1.377
Cirque	ULB	ULB-13	53.17785	-6.29823	471	Boulder	42.77	0.80	13.409	1.378
Cirque	ULB	ULB-14	53.17756	-6.29822	471	Boulder	43.34	0.96	13.086	1.378
Cirque	ULB	ULB-15	53.17737	-6.29801	471	Boulder	45.53	0.69	11.846	1.381
Cirque	ULB	ULB-16	53.17711	-6.29775	471	Boulder	42.88	0.93	13.345	1.378
Cirque	ULB	ULB-17	53.17694	-6.29753	471	Boulder	39.79	0.78	15.1	1.376
Cirque	ULB	ULB-18	53.17675	-6.29755	463	Boulder	43.86	0.93	12.79	1.379
Cirque	ULB	ULB-19	53.17635	-6.29698	460	Boulder	38.29	0.69	15.951	1.376
Cirque	ULB	ULB-20	53.17632	-6.29698	459	Boulder	43.10	0.70	13.231	1.378
Valley	LB	LB-01	53.07045	-6.35507	394	Boulder	37.26	1.04	16.538	1.377
Valley	LB	LB-02	53.07046	-6.35512	393	Boulder	38.69	0.93	15.726	1.376
Valley	LB	LB-03	53.07034	-6.35513	395	Boulder	37.59	0.95	16.345	1.377
Valley	LB	LB-04	53.07009	-6.35499	396	Boulder	39.72	1.05	15.137	1.376
Valley	LB	LB-05	53.07006	-6.355	396	Boulder	37.93	0.90	16.156	1.377
Valley	LB	LB-06	53.07009	-6.35495	396	Boulder	39.43	0.72	15.302	1.376
Valley	LB	LB-07	53.07003	-6.35471	396	Boulder	38.44	0.97	15.874	1.376
Valley	LB	LB-08	53.07015	-6.3546	396	Boulder	38.71	0.90	15.715	1.376
Valley	LB	LB-09	53.07041	-6.35415	390	Boulder	38.44	1.00	15.862	1.376
Valley	LB	LB-10	53.07045	-6.35399	390	Boulder	40.34	0.82	14.791	1.376
Valley	LB	LB-11	53.07029	-6.35407	392	Boulder	38.82	0.94	15.656	1.376
Valley	LB	LB-12	53.0702	-6.35389	393	Boulder	39.35	0.68	15.357	1.376
Valley	LB	LB-13	53.07032	-6.35356	393	Boulder	39.02	0.89	15.543	1.376
Valley	LB	LB-14	53.07028	-6.35348	394	Boulder	38.06	0.65	16.091	1.376

Valley	LB	LB-15	53.07027	-6.35349	394	Boulder	37.20	1.11	16.57	1.377
Valley	LB	LB-16	53.07012	-6.35328	394	Boulder	39.07	0.80	15.52	1.376
Valley	LB	LB-17	53.07022	-6.35302	391	Boulder	39.17	0.92	15.454	1.376
Valley	LB	LB-18	53.06963	-6.35252	395	Boulder	39.37	0.93	15.34	1.376
Valley	LB	LB-19	53.06958	-6.35199	389	Boulder	39.14	1.13	15.469	1.376
Valley	LB	LB-20	53.06971	-6.35162	384	Boulder	39.48	0.79	15.281	1.376
Valley	CB	CB-01	52.96432	-6.40324	423	Boulder	39.52	0.66	15.264	1.376
Valley	CB	CB-02	52.96429	-6.40317	424	Boulder	39.79	0.79	15.113	1.376
Valley	CB	CB-03	52.9643	-6.40319	423	Boulder	38.20	0.69	16.021	1.376
Valley	CB	CB-04	52.96428	-6.4031	421	Boulder	39.36	0.64	15.359	1.376
Valley	CB	CB-05	52.96423	-6.40311	421	Boulder	40.53	0.54	14.696	1.376
Valley	CB	CB-06	52.96421	-6.40317	421	Boulder	38.91	0.80	15.616	1.376
Valley	CB	CB-07	52.96425	-6.40302	420	Boulder	38.84	0.79	15.656	1.376
Valley	CB	CB-08	52.96436	-6.4029	420	Boulder	36.25	0.70	17.112	1.378
Valley	CB	CB-09	52.96431	-6.40291	419	Boulder	39.22	0.76	15.431	1.376
Valley	CB	CB-10	52.96418	-6.40294	418	Boulder	38.79	0.90	15.662	1.376
Valley	UGD	UGD-01	53.02901	-6.36507	336	Boulder	38.23	0.93	15.984	1.376
Valley	UGD	UGD-02	53.02903	-6.36502	336	Boulder	37.90	0.91	16.173	1.377
Valley	UGD	UGD-03	53.02916	-6.36542	332	Boulder	39.77	0.90	15.113	1.376
Valley	UGD	UGD-04	53.02936	-6.3655	330	Boulder	39.07	0.90	15.51	1.376
Valley	UGD	UGD-05	53.02939	-6.36557	330	Boulder	38.21	0.96	16.002	1.376
Valley	UGD	UGD-06	53.0296	-6.36602	333	Boulder	37.71	0.73	16.286	1.377
Valley	UGD	UGD-07	53.0297	-6.36598	335	Boulder	39.89	0.97	15.054	1.376
Valley	UGD	UGD-08	53.02973	-6.36654	328	Boulder	40.46	0.97	14.731	1.376
Valley	UGD	UGD-09	53.02976	-6.36657	329	Boulder	37.25	0.91	16.551	1.377
Valley	UGD	UGD-10	53.02974	-6.36667	328	Boulder	36.75	0.68	16.835	1.377
Valley	UGD	UGD-11	53.03012	-6.36654	334	Boulder	36.35	0.84	17.062	1.378
Valley	UGD	UGD-12	53.0302	-6.36666	332	Boulder	36.26	0.78	17.115	1.378
Valley	UGD	UGD-13	53.03029	-6.36672	333	Boulder	39.81	0.71	15.098	1.376
Valley	UGD	UGD-14	53.03049	-6.36659	332	Boulder	38.94	0.82	15.586	1.376
Valley	UGD	UGD-15	53.03056	-6.36662	332	Boulder	37.61	0.99	16.351	1.377
Valley	UGD	UGD-16	53.03062	-6.36666	330	Boulder	39.21	1.03	15.423	1.376
Valley	UGD	UGD-17	53.03066	-6.36667	330	Boulder	39.29	0.96	15.385	1.376

Valley	UGD	UGD-18	53.03097	-6.367	330	Boulder	37.58	0.93	16.358	1.377
Valley	UGD	UGD-19	53.03113	-6.3668	337	Boulder	39.93	1.12	15.022	1.376
Valley	UGD	UGD-20	53.03128	-6.36709	334	Boulder	38.19	0.83	16.008	1.376
Valley	GW	GW-01	53.06269	-6.33445	275	Boulder	37.29	0.97	16.498	1.377
Valley	GW	GW-02	53.06269	-6.3345	274	Boulder	38.13	0.86	16.021	1.376
Valley	GW	GW-03	53.0626	-6.33461	273	Boulder	38.36	1.09	15.891	1.376
Valley	GW	GW-04	53.06254	-6.33465	269	Boulder	39.13	0.95	15.454	1.376
Valley	GW	GW-05	53.06248	-6.33472	266	Boulder	35.67	0.72	17.422	1.378
Valley	GW	GW-06	53.06242	-6.33468	271	Boulder	36.61	0.83	16.892	1.377
Valley	GW	GW-07	53.06235	-6.33471	270	Boulder	36.35	0.90	17.044	1.378
Valley	GW	GW-08	53.06227	-6.33476	267	Boulder	38.18	1.01	16.002	1.376
Valley	GW	GW-09	53.0622	-6.3347	266	Boulder	35.92	0.81	17.29	1.378
Valley	GW	GW-10	53.06211	-6.33465	268	Boulder	36.22	0.81	17.119	1.378
Valley	GW	GW-11	53.06207	-6.33459	268	Boulder	37.16	1.06	16.589	1.377
Valley	GW	GW-12	53.06197	-6.33464	269	Boulder	36.73	1.00	16.835	1.377
Valley	GW	GW-13	53.06182	-6.3347	269	Boulder	37.43	0.94	16.438	1.377
Valley	GW	GW-14	53.06169	-6.3347	268	Boulder	36.50	0.78	16.968	1.378
Valley	GW	GW-15	53.06165	-6.33473	267	Boulder	37.27	0.86	16.532	1.377
Valley	GW	GW-16	53.06153	-6.33473	268	Boulder	37.14	0.79	16.608	1.377
Valley	GW	GW-17	53.06144	-6.33487	266	Boulder	37.98	0.74	16.135	1.377
Valley	GW	GW-18	53.0614	-6.33493	262	Boulder	36.98	0.79	16.703	1.377
Valley	GW	GW-19	53.06132	-6.33491	261	Boulder	37.72	0.88	16.286	1.377
Valley	GW	GW-20	53.0612	-6.33494	261	Boulder	37.92	0.61	16.173	1.377
Summit	CS	CS-01	53.08641	-6.3626	570	Bedrock	35.45	0.63	17.56	1.379
Summit	CS	CS-02	53.08638	-6.36257	571	Boulder	34.01	0.58	18.389	1.381
Summit	CS	CS-03	53.08649	-6.36254	570	Bedrock	35.62	0.73	17.464	1.378
Summit	CS	CS-04	53.08645	-6.36234	570	Bedrock	39.11	0.82	15.478	1.376
Summit	CS	CS-05	53.08653	-6.36226	570	Bedrock	39.31	0.80	15.367	1.376
Summit	CS	CS-06	53.08663	-6.36216	570	Boulder	37.31	1.00	16.506	1.377
Summit	CS	CS-07	53.0864	-6.36238	570	Bedrock	39.39	0.66	15.321	1.376
Summit	CS	CS-08	53.08634	-6.36248	570	Bedrock	36.21	0.81	17.127	1.378
Summit	CS	CS-09	53.08615	-6.36222	569	Bedrock	39.03	0.56	15.529	1.376
Summit	CS	CS-10	53.08611	-6.36223	569	Bedrock	40.13	0.75	14.905	1.376

Summit	CS	CS-11	53.08605	-6.36221	567	Bedrock	38.09	0.50	16.059	1.376
Summit	CS	CS-12	53.08595	-6.36209	567	Boulder	37.23	1.02	16.548	1.377
Summit	CS	CS-13	53.08597	-6.36204	568	Bedrock	39.01	0.81	15.548	1.376
Summit	CS	CS-14	53.086	-6.3619	568	Bedrock	39.58	0.70	15.226	1.376
Summit	CS	CS-15	53.08591	-6.3618	568	Bedrock	36.97	0.94	16.703	1.377
Summit	CS	CS-16	53.08586	-6.36144	569	Bedrock	36.74	0.79	16.835	1.377
Summit	CS	CS-17	53.08616	-6.36171	569	Bedrock	36.67	0.71	16.871	1.377
Summit	CS	CS-18	53.08634	-6.36132	569	Boulder	37.58	0.99	16.353	1.377
Summit	CS	CS-19	53.08645	-6.36164	569	Boulder	37.25	0.73	16.544	1.377
Summit	CS	CS-20	53.08644	-6.36157	569	Bedrock	37.66	0.80	16.317	1.377

[a] Standard Error of the Mean